O_2 Adsorption Dynamics at Metal Surfaces: Non-Adiabatic Effects, Dissociation and Dissipation

Christian Carbogno, Axel Groß, Jörg Meyer, and Karsten Reuter

1 Introduction

Without doubt the interaction of oxygen with metal surfaces is of tremendous technological importance in, e.g., heterogeneous and electro-catalysis or corrosion [1]. However, also on a conceptual level the oxygen-metal interaction is a multi-faceted and highly challenging topic: Next to H_2 at metal surfaces, dioxygen is often viewed as the "next higher level of complexity" in studying gas-surface interaction and gas-surface dynamics. While this increase in complexity when changing from one first-row diatomic to one from the second row might seem marginal at first glance, there are in fact several issues that already each alone, but even more so when combined, render in particular its quantitative theoretical description a still in parts elusive hallmark: To begin with, the quenching of the spin-triplet ground state of gas-phase O_2 into a singlet state upon adsorption at most metal surfaces is governed by strict spin-selection rules, which give rise to a complex spin-flip dissociation dynamics that is inherently non-adiabatic. An appropriate account of concomitant spin-transitions (or their absence) or strong electron-hole pair excitation in the high-dimensional surface dissociation process is thus already a first cornerstone that needs to be mastered. As a second ingredient the potential energy surfaces (PESs) underlying this process can

Christian Carbogno
Fritz-Haber-Institut der Max-Planck-Gesellschaft, D-14195 Berlin, Germany, e-mail: christian.carbogno@fhi-berlin.mpg.de

Axel Groß
Institut für Theoretische Chemie, Universität Ulm, D-89069 Ulm, Germany, e-mail: axel.gross@uni-ulm.de

Jörg Meyer
Lehrstuhl für Theoretische Chemie, Technische Universität München, D-85747 Garching, Germany, e-mail: joerg.meyer@ch.tum.de

Karsten Reuter
Lehrstuhl für Theoretische Chemie, Technische Universität München, D-85747 Garching, Germany, e-mail: karsten.reuter@ch.tum.de

be considerably more complex as e.g. compared to those for H_2 at metals, owing to the π-orbital involving chemical bond of O_2. The contracted, localized character of the O_2 orbitals represents furthermore still a significant challenge to contemporary first-principles electronic structure theories, which for the surface dissociation process need to simultaneously describe the delocalized metal electrons in appropriate large supercell geometries. Last, but not least, O_2 dissociation at most metal surfaces is a highly exothermic process, releasing typically several electron volts that need to be dissipated into the system. This is a staggering amount of energy in light of the two major dissipation channels, e-h pairs and phononic degrees of freedom. To account for the latter of the two, at least the substrate motion in the immediate vicinity of the impact point needs to be included in the modeling, coupled to some appropriate form of heat sink to also correctly describe the adsorbate dynamics ensuing the dissociation.

In spite of all these problems and challenges, there has recently been significant progress in the detailed description and understanding of the O_2 adsorption dynamics on metal surfaces. In this chapter, we will review this progress, using case studies primarily from our own work to illustrate the aforementioned major issues in the O_2 adsorption process. Much of the understanding with respect to the spin flip dynamics has evolved around the O_2 at Al(111) system, where only an explicit account of the suppressed triplet-singlet transition could reconcile first-principles dynamical simulations with the experimentally measured low sticking coefficient for thermal molecules. This non-adiabatic hindrance is particularly pronounced at the Al(111) surface due to the inefficiency of both coupling mechanisms generally discussed to relax the spin selection rules: The low mass number of Al leads to a small spin-orbit coupling and the low Al density of states (DOS) at the Fermi level prevents efficient spin quenching through the tunneling of electrons between substrate and adsorbate. Once understood, this obviously dictates trend studies involving substrates with higher mass number and/or higher Fermi-level DOS to disentangle the two mechanisms. In this respect we will proceed with a discussion of corresponding work that has addressed the O_2 dissociation at a heavier transition metal surface, namely Pd(100).

The intricate adsorption dynamics resulting from the PES complexity is prototypically highlighted by work at the Pt(111) surface. Here, oxygen molecular physisorption and chemisorption as well as atomic adsorption states exist. The actual adsorption process proceeds then typically in two steps, where the O_2 molecules first become trapped in molecular chemisorption states, and only then the molecules dissociate due to thermal fluctuations. These details can, of course, only be captured by explicit dynamical simulations, which reveal the energy transfer between the different degrees of freedom. For initial trapping as at Pt(111) the crucial transfer is predominantly the one into O_2 internal degrees of freedom (vibrational excitation). For the ensuing dissociation process with its concomitant enormous energy release the transfer into substrate degrees of freedom instead becomes the central aspect. Obviously, the efficiency with which this transfer into either e-h pairs or phononic excitations occurs sensitively determines the adsorbate dynamics at and after the dissociation point. This and the longer term energy dissipation into a realistic metal

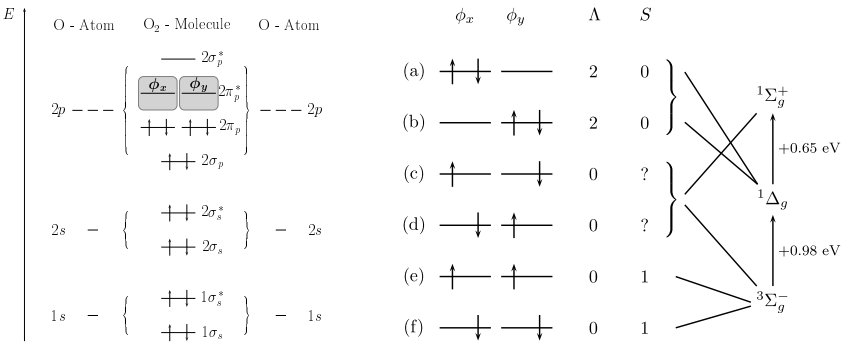

Fig. 1 The left sketch shows the O_2's molecular orbitals (MOs) in energetic order as obtained from the symmetric and antisymmetric combination of the single oxygen's orbitals. All MOs up to the two-fold degenerate $2\pi_p$ orbitals are completely filled, whereas the two-fold degenerate, gray shaded anti-bonding $2\pi_p^*$ orbitals are half filled. The resulting six possible configurations for these valence orbitals are shown on the right, whereby the quantum numbers of the projected angular momentum Λ and of the total spin S are also given if possible. Finally, the pairs of determinants which have to be combined to yield correct electronic states are also denoted.

bulk has first been analyzed in detail for O_2 at Pd(100), which already by itself demonstrates again the intriguing richness of novel aspects that appear when simply moving "from one diatomic to another".

2 The Free Oxygen Molecule

It is a well-known fact that the O_2 molecule plays a prominent role in the circle of life as a highly available oxidation partner. Noteworthy enough though, it behaves rather inert in the gas-phase in spite of its open-shell triplet (diradical) character, if the other reactant and the product are spin singlets. The reason for this behavior is the constraint of overall spin conservation as first formulated by Wigner [2]. To clarify this point, we will first discuss the electronic ground and excited states of O_2 qualitatively in terms of *molecular orbitals* (MOs). In a second step, we will then discuss the ability of quantum chemical and density-functional theory (DFT) methods to describe these electronic states and so to reproduce the experimental measurements.

The electronic configuration of a single oxygen atom is $1s^2 2s^2 2p^4$, which according to Hund's rules [3] leads to a ^3P ground state. In an oxygen molecule, the respective atomic orbitals couple to bonding and anti-bonding MOs (see Fig. 1). For the energetically lowest electronic states of the O_2 molecule all MOs up to the $2\pi_p^*$ level are completely filled, while the $2\pi_p^*$ MOs that comprise the two degenerate orbitals $\phi_x \sim 2p_x - 2p_x$ and $\phi_y \sim 2p_y - 2p_y$ are half filled. As shown schematically in Fig. 1, there are six distinct possibilities to arrange the two residual valence electrons in these $2\pi_p^*$ orbitals. The correct molecular wave functions must, however,

be an eigenfunction of the angular momentum $\mathbf{L}^2$ and of the spin momentum operator $\mathbf{S}^2$ as well. To fulfill this condition, the wave function must for instance not change when any two antiparallel spins are pairwise flipped in the valence orbitals. This so called *static correlation* is accounted for in the pairwise symmetric and antisymmetric combinations of the individual Slater determinants, which eventually yield the correct wave functions for the oxygen molecule[1]:

$$\text{a)}\ {}^1\Delta_g:\ \Psi_1^s = \frac{1}{2}\left(\phi_x\phi_x - \phi_y\phi_y\right)\left(|\uparrow\downarrow\rangle - |\downarrow\uparrow\rangle\right) \tag{1}$$

$$\text{b)}\ {}^1\Delta_g:\ \Psi_2^s = \frac{1}{2}\left(\phi_x\phi_x + \phi_y\phi_y\right)\left(|\uparrow\downarrow\rangle - |\downarrow\uparrow\rangle\right) \tag{2}$$

$$\text{c)}\ {}^1\Sigma_g^+:\ \Psi_3^s = \frac{1}{2}\left(\phi_x\phi_y + \phi_y\phi_x\right)\left(|\uparrow\downarrow\rangle - |\downarrow\uparrow\rangle\right) \tag{3}$$

$$\text{d)}\ {}^3\Sigma_g^-:\ \Psi_4^t = \frac{1}{2}\left(\phi_x\phi_y - \phi_y\phi_x\right)\left(|\uparrow\downarrow\rangle + |\downarrow\uparrow\rangle\right) \tag{4}$$

$$\text{e)}\ {}^3\Sigma_g^-:\ \Psi_5^t = \frac{1}{\sqrt{2}}\left(\phi_x\phi_y - \phi_y\phi_x\right)|\uparrow\uparrow\rangle \tag{5}$$

$$\text{f)}\ {}^3\Sigma_g^-:\ \Psi_6^t = \frac{1}{\sqrt{2}}\left(\phi_x\phi_y - \phi_y\phi_x\right)|\downarrow\downarrow\rangle \tag{6}$$

As long as spin-orbit coupling is neglected, these six wave functions correspond to **three** energetically distinct electronic states: the threefold degenerate triplet ground state ${}^3\Sigma_g^-$, the twofold degenerate first excited singlet state ${}^1\Delta_g$ that is experimentally found to be 0.975 eV higher in energy [4], and the second excited singlet state ${}^1\Sigma_g^+$, 1.624 eV above the ground state [4].

As shown above, the ${}^1\Delta_g$ and ${}^1\Sigma_g^+$ state of the oxygen molecule are represented by the superposition of **two** Slater Determinants – even in the independent electron, molecular orbital picture. Such electronic configurations are typically referred to as *multi-reference* states. The resulting *static correlation* is not well described by common functionals of DFT [5], as highlighted by the fact that the singlet ${}^1\Delta_g$ and ${}^1\Sigma_g^+$ states as well as the low-spin ${}^3\Sigma_g^-$ state exhibit the exact same electronic and magnetization densities.

2.1 First-principles Calculations of the Free Oxygen Molecule

Determining the properties of even an isolated oxygen molecule thus represents already a significant challenge to first-principles electronic structure techniques. This is illustrated in Tab. 1, were quantum chemical calculations at different levels of theory are compared with experiment. In detail, the following *ab initio* wave-function based methods have been employed: *Unrestricted Hartree-Fock* (UHF), *Restricted Open-Shell HF* (ROHF), *Multi-configuration Self-Consistent Field* (MCSCF) with

[1] The usual shortened textbook notation $\phi_x\phi_y|\uparrow\downarrow\rangle = \phi_x(1)\phi_y(2)|\uparrow(1)\rangle|\downarrow(2)\rangle$ has been employed.

the smallest number of Slater determinants compatible with the symmetry of the electronic state, *Complete Active Space SCF* (CASSCF) with fully occupied $1\sigma_s$ and $1\sigma_s^*$ states as well as fixed spin and orbital momentum, *Full Valence Configuration Interaction* (FVCI) [6], *CI with Single and Double Excitations* (CISD) with "frozen" core $1\sigma_s$ and $1\sigma_s^*$ orbitals and Multi-Reference CISD (MRCI) calculations, for which the CASSCF wave functions served as a reference. Furthermore, results of DFT calculations with various (semi-)local exchange-correlation (xc) functionals (LDA [7], PW91 [8], PBE [9], RPBE [10]) are included.

The equilibrium oxygen-oxygen distance d_{eq} is already well-reproduced using the single-determinant Hartree-Fock methods. This is not too surprising due to the single determinant character of the O_2 ground state. The vibrational frequency shows a larger relative error due to its higher sensitivity on the shape of the potential energy curve (PEC) away from the minimum. The stepwise introduction of further correlation in the FVCI, CISD, CASSCF and MRCI methods yields almost perfect agreement with the experimental data though. This is, however, not the case for the binding energy E_{b}, which is also listed in Tab. 1. Pure Hartree-Fock methods fail dramatically – predicting a binding energy almost 4 eV lower than the experimental value. Even the more sophisticated methods do not yield "chemical accurate" results. A large portion of this error in the computed binding energy is caused by the lack of size consistency in truncated CI methods [15], as can be seen from the binding energy determined with respect to two oxygen atoms at large distance (MRCI PEC). Yet, even when accounting for such effects, an accurate reproduction of the experimental binding energy can only be achieved via the inclusion of higher order excitations [16].

Method	d_{eq} (Å)	ω_o(cm $^{-1}$)	E_{b} (eV)	$\Delta E_{\mathrm{TS}}^{\Delta}$ (eV)	$\Delta E_{\mathrm{TS}}^{\Sigma}$ (eV)
UHF	1.153	2002	-1.441	2.323	–
ROHF	1.146	2045	-1.195	1.722	–
MCSCF	1.146	2045	-1.195	1.286	2.549
CASSCF	1.213	1540	-3.909	0.956	1.477
FVCI	1.177	1808	-3.857	1.095	1.953
CISD	1.187	1718	-4.098	0.923	1.576
MRCI	1.204	1586	-4.564	0.961	1.612
MRCI (PEC)	–	–	-4.933	–	–
DFT, LDA	1.218	1632	-7.258	1.016	
DFT, PW91	1.230	1565	-6.038	1.090	
DFT, PBE	1.230	1565	-5.945	1.125	
DFT, RPBE	1.232	1550	-5.574	1.155	
experiment [11]	1.207	1580	-5.116	–	–
experiment [12]	–	–	-5.123	–	–
experiment [4]	–	–	–	0.975	1.624
experiment [13]	–	–	–	0.981	–

Table 1 Calculated equilibrium molecular bond lengths d_{eq}, vibrational frequencies ω_o and binding energies E_{b} of the O_2 molecule in its $^3\Sigma_g^-$ ground state at different levels of theory. The excitation energies for the $^1\Delta_g$ and $^1\Sigma_g^+$ states are listed in the two rightmost columns. All calculational details can be found in Ref. [14].

In light of these facts it might seem surprising that DFT is able to reproduce the basic structural properties d_{eq} and ω_o of the oxygen molecule quite satisfactorily even at the (semi-)local level of theory. A far too high binding energy is, however, predicted by the DFT calculations: The LDA result is off by more than 2 eV, the PW91 and PBE calculations by ~ 1 eV. Not too surprisingly, the best agreement with experiment is achieved with the RPBE functional [10], i.e., a slightly altered version of the PBE functional. In this particular GGA-functional the functional form of the *exchange enhancement factor* is modified to reproduce *Optimized Exchange Potential* simulations [17] for a variety of elements including oxygen [18] while still fulfilling the local Lieb-Oxford inequality [19] for all generalized gradients [10]. Still, even this "optimized" functional exhibits an error of ~ 0.5 eV in the binding energy.

The problem gets even more complex for the excited singlet states: As discussed in the introduction, multiple determinants are actually required in the simulation of the ${}^1\Delta_g$ and ${}^1\Sigma_g^+$ states; hence the single determinant Hartree-Fock methods cannot yield correct results by construction. Accordingly, the resulting triplet-singlet gap $\Delta E_{\mathrm{TS}}^{\Delta}$ is by far too large in the UHF and ROHF methods due to the additional electrostatic repulsion induced by forcing the electrons to occupy either the ϕ_x or the ϕ_y orbital. Often in HF routines, the ${}^1\Sigma_g^+$ state is not accessible at all, since the single Slater determinants that would exhibit the correct symmetries are not eigenfunctions of the total spin operator [14]. Naturally, this problem can be overcome in multi-reference methods, whereby the inclusion of further correlations eventually leads to an almost perfect agreement between experiment and the MRCI calculations. The inclusion of multiple reference states is not straightforwardly possible in DFT calculations, though. Nevertheless, the excited singlet states can be accessed in DFT by reverting to the *spin-unpolarized* formulation of DFT, in which a "closed-shell" configuration is inherently enforced. Obviously, such an occupation pattern cannot be achieved by distributing the two available valence electrons on the four accessible $2\pi^*$ states. By means of *fractional occupation numbers* [20] such a configuration can nevertheless be obtained. In this case, each of the available states in the ϕ_x and ϕ_y molecular orbitals is occupied with **half** an electron, which results in a superposition of the ${}^1\Delta_g$ and ${}^1\Sigma_g^+$ states. Accordingly, the DFT calculations (see Tab. 1) cannot discriminate between the two singlet states and thus will never yield the correct, lower lying ${}^1\Delta_g$ state [21].

2.2 Transition Probabilities and Lifetimes

As the triplet-singlet transition is a central feature of the O_2 dissociation process at metal surfaces, let us further analyze the lifetimes of the two excited singlet states of gas-phase O_2 in some more detail. Radiative decay from the lower-lying singlet states into the ground state is strongly suppressed due to the $\Delta S = 0$ selection rule that applies to all electromagnetic transitions. Additionally, restrictions for $\Delta \leftrightarrow \Sigma$ and for parity preserving $g \nleftrightarrow u$ transitions exist as well [11]. These selection rules

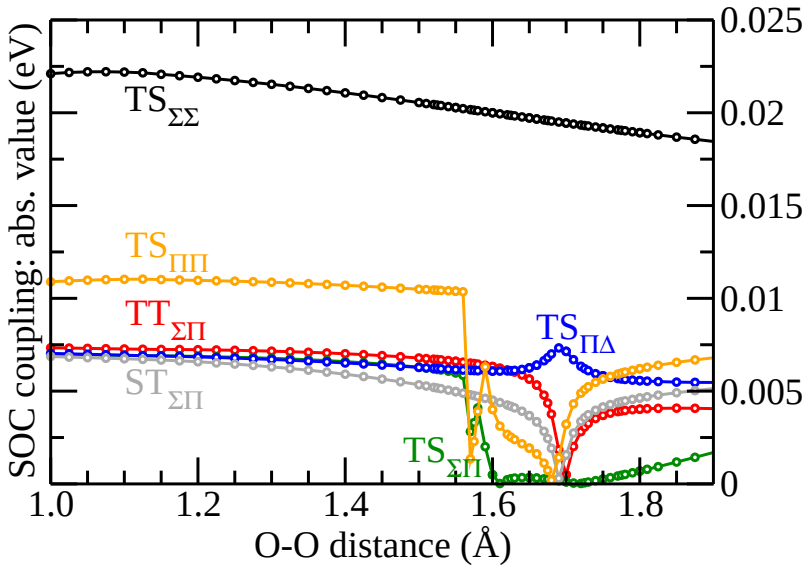

Fig. 2 Absolute values of the triplet-triple (TT), triplet-singlet (TS) and singlet-triplet (ST) spin-orbit coupling matrix elements for the ${}^3\Sigma_g^-$, ${}^1\Delta_g$, ${}^1\Sigma_g^+$, ${}^3\Pi_g$, ${}^1\Pi_g$ states of the oxygen molecule. The single data points are separated by 0.025 Å from each other for oxygen-oxygen distances smaller than 1.5 Å and by 0.01 Å for larger distances.

result in experimental lifetimes of about 12 seconds [22] for the ${}^1\Sigma_g^+$ state and of 72 minutes [4] for the ${}^1\Delta_g$ state in the gas phase. The latter transition is correspondingly often referred to as the *most forbidden transition in nature* [23]. Notwithstanding, "most forbidden" does not mean completely forbidden: As a matter of fact, spin-orbit coupling V_{SOC} leads to a (minute) mixing of states with different multiplicity and thus to a partial invalidation of the $\Delta S = 0$ selection rule. In a simplified first-order perturbation type picture, the lifetime can be estimated by evaluating the spin-orbit coupling matrix elements and relating them to the experimental energy gaps ΔE_{TS}^{Σ}. A less approximative assessment of these coefficients can be performed by diagonalizing the complete interaction matrix for the spin-orbit coupling [24]. The absolute values of these matrix elements are plotted in Fig. 2. As shown there, the coupling of the ${}^3\Sigma_g^-$ state to the ${}^1\Sigma_g^+$ state is a slightly decreasing, almost constant function of the oxygen-oxygen distance. In contrast thereto, all other matrix elements exhibit more or less strong wiggles for distances larger than 1.6 Å. These oscillations and discontinuities are caused by the avoided crossings of the respective Π states, to which all these matrix elements couple.

Since the spin-orbit coupling mixes states with different multiplicity, but not states with different inversion symmetry, electric dipole transitions from the ${}^1\Sigma_g^+$ or the ${}^1\Delta_g$ state to the triplet ${}^3\Sigma_u^+$ ground state are still forbidden due to the $g \leftrightarrow u$ selection rule. The next possible, parity preserving transition mechanism is the *magnetic*

dipole operator

$$\mathbf{M} = \frac{\mu_B}{\hbar}\left(\mathbf{L} + g_e\mathbf{S}\right) \tag{7}$$

which leads to inverse lifetimes

$$\frac{1}{\tau} = \frac{\alpha^5\omega^3\bar{h}^2 f}{3\mu_B^2}\left|\langle\Psi_{\text{ini}}|\,\mathbf{M}\,|\Psi_{\text{fin}}\rangle\right|^2 , \tag{8}$$

in which μ_B denotes the Bohr magneton, g_e the gyromagnetic *g-factor* for the electron, α the fine-structure constant, ω the transition frequency, f the degeneracy of the final state and Ψ_{ini}, Ψ_{fin} the initial and final state, respectively. For both the $^1\Sigma_g^+$ and the $^1\Delta_g$ state, applying this expression to high-level theory matrix elements leads to lifetimes in excellent agreement with experiment [4, 25], as illustrated in Table 2.

3 Electronically non-adiabatic adsorption dynamics

The ground-state oxygen molecule with its peculiar electronic structure featuring two unpaired electrons represents a diradical. Typically, such species are known to exhibit a high reactivity. Still, in spite of the fact that the atmosphere consists to 20 percent of this thus nominally reactive species oxygen, air seems to be relatively inert. This is due to the discussed spin selection rules, which lead to a weak interaction of the triplet oxygen with matter that is predominantly in the singlet state. Since the spin transition from triplet to singlet oxygen is typically strongly suppressed, the oxygen molecule often remains in its triplet state when interacting with matter, even if a spin transition results in an energetically more favorable state. Obviously, one may suspect that this must also have direct consequences on the actual interaction dynamics of O_2 molecules with metal surfaces – unless there are other mechanisms that efficiently quench the spin-flip limitations. As kind of an evergreen in the gas-surface dynamics community a critical role of corresponding electronically non-adiabatic effects has in fact been conjectured for many surfaces. Probably

τ_Σ (s)	Reference	
11.16	MRCI	[14]
11.11	MRCI, exp. ΔE_{TS}^{Σ}	[14]
11.24	experiment	[22]
11.3	experiment	[4]
11.65	MRCI	[26]
12.59	CASSCF, linear response	[27]

τ_Δ (s)	Reference	
5799.30	MRCI	[14]
5542.48	MRCI, exp. ΔE_{TS}^{Δ}	[14]
3875.96	experiment	[28]
4347.82	experiment	[25]
5271.48	MRCI	[26]
5263.16	MRCI	[29]

Table 2 Lifetimes τ_Σ and τ_Δ for the $^1\Sigma_g^+$ and the $^1\Delta_g$ state, respectively: All values refer to the decay in the triplet ground state. Additionally, lifetimes calculated by employing the experimental energy gaps are given.

the system for which such effects have been most intensively studied (but still not completely validated) is the dissociative adsorption of oxygen at Al(111), which is why we begin our survey with this particular system.

3.1 Dissociative Adsorption of Oxygen on Aluminum(111): Hindered Spin-Transition

The initial oxidation of the lowest-energy (111) surface of aluminum exhibits quite a number of peculiar features that have puzzled researchers over the last decades. First and foremost, experimental findings [30] show that the dissociative adsorption probability at the clean aluminum surface is approximately 1% at room temperature, but no state-of-the-art adiabatic theory has yet found any indications for a corresponding activated nature of the O_2-Al(111) interaction. Such severe discrepancy between theory and experiment for such an elemental process is rather alarming: Clearly, only a theory that correctly reproduces and explains the low initial adsorption probability S_0 of thermal oxygen molecules can serve as a basis for further studies of more complex phenomena, such as the dynamics of the individual oxygen atoms closer to or at the surface [31, 32, 33].

As shown in Fig. 3 the experimentally measured initial sticking coefficient S_0 exhibits a typical "S"-shape [30]. This fact strongly suggests that the underlying dynamics is *activated* [34], i.e. that **each** possible pathway towards dissociation is energetically hindered by a barrier on the respective PES. However, an almost complete absence of barriers has been found in theoretical investigations based upon adiabatic semi-local DFT methods [35, 36]. As a consequence, molecular dynamics simulations on such adiabatic PESs yield a constant sticking coefficient of 100% even for thermal molecules, as shown in Fig. 3. In view of the discussed spin-selection rules a possible explanation for this dramatic discrepancy between experiment and theory is the occurrence of non-adiabatic spin-flips in the dissociation dynamics. Whereas the initially separated molecule-surface system is in an overall spin triplet state, the oxidized surface is in an overall spin singlet state, so that a spin-transition must occur along the pathway of the oxygen molecule. If spin selection rules are as discriminating in this process as they are for transitions in the gas phase (see Sec. 2.2), the overall spin configuration cannot relax into a singlet state as soon as this becomes energetically favorable during the adsorption process (see Fig. 3). To model such a limitation, Behler *et al.* [37, 38] calculated a "triplet PES" for this system, by enforcing a constant number and spin alignment of the oxygen electrons through a constrained DFT approach. On this special PES, barriers are present for each possible pathway towards dissociation and respective molecular dynamics simulations relying on this potential yield indeed an "S"-shaped sticking coefficient (see Fig. 3).

While encouraging in their agreement with the experimental data, this approach provides, of course, only an indirect evidence for the relevance of spin-transitions. Furthermore, the chosen spin-triplet-only model for the description of the reac-

tion is intrinsically flawed, since the oxygen molecule can never reach the correct final spin-singlet state. To overcome this limitation and so to directly include non-adiabatic spin-flip transitions in the description of the reaction, Carbogno *et al.* [39, 40] continued on this approach and performed mixed quantum-classical (MQC) simulations for the dynamics on multiple potential energy surfaces in terms of *Tully's Fewest Switches Surface Hopping* algorithm [41]. In principle, the study of such non-adiabatic effects would require a concurrent quantum treatment of both the electronic and the nuclear degrees of freedom. Such a full quantum approach is, however, computationally prohibitively costly in the description of adsorption processes on surfaces. For the investigation of non-adiabatic effects in molecule-surface processes [42, 43], mixed quantum-classical *Surface Hopping* algorithms [41, 44, 45] represent instead a viable and accurate alternative at a fraction of the computational cost: In these approaches, the nuclei are typically treated classically, i.e., they move on **one** PES (associated to **one** distinct electronic state) in each time step. As it is the case in traditional molecular dynamics (MD) algorithms, the classical trajectory of the nuclei is thus determined by stepwise numerical integration of the Newtonian equations of motion. In *Surface Hopping* algorithms, the evolution of the *density matrix* for **all** electronic states associated to a PES is determined on top of that by integrating the time-dependent Schrödinger Equation for this multi-level system along the classical trajectory of the nuclei. The thereby computed diagonal elements of the electronic density matrix, i.e., the occupation numbers of the individual electronic states, allow the introduction of physically motivated transitions between the various PESs. When such a "switch" takes place, the PES associated to the new electronic state will determine the classical motion of the nuclei for all subsequent time steps – until the next "switch" occurs. In *Tully's Fewest Switches* algorithm, which is one of the most wide-spread and successful *Surface Hopping* methods, such "switches" are carried out randomly under the constraint [41] that the correct statistical distribution of state populations given by the occupation numbers is maintained at all times with as few switches as possible.

Carbogno *et al.* utilized this algorithm to clarify the role of non-adiabatic spin-flips in the dissociative adsorption of oxygen on the (111) surface of aluminum. By including not only the aforementioned "triplet" PES, but also a "singlet" PES [37, 38] in these mixed quantum-classical (MQC) simulations, they were able to correctly describe both the initial and the final state of the reaction, as shown in Fig. 3. An accurate description of the electronic transitions is hereby achieved by deriving a lower and an upper bound ($V_{\mathrm{min}}/V_{\mathrm{max}}$) for the electronic coupling between the triplet and the singlet state V_{ts} from first-principles calculations of the spin-orbit coupling of an isolated O_2-molecule [40] and from the adiabatic PES [39], respectively.

As shown in Fig. 3, such MQC simulations of the sticking coefficient at normal incidence lead to the same qualitative behavior as found before by Behler *et al.* [37, 38] with classical MD simulations on the "triplet" PES alone: At small incident energies, non-adiabatic spin-flips play no role at all, since the molecules are repelled on the "triplet" PES before being able to reach the triplet-singlet crossing seam. At medium incident energies, a notably larger dissociation probability is found in the MQC simulations compared to MD though. Molecules that would not

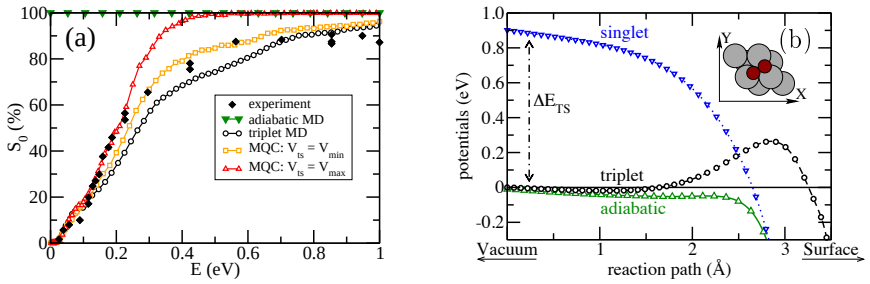

Fig. 3 The left plot shows the sticking coefficient S_0 as computed by molecular dynamics (MD) on the adiabatic and on the triplet potential energy surface and by mixed quantum-classical (MQC) simulations for the minimal and maximal coupling, respectively. The respective experimental data [30] is shown as well. The right figure shows the minimum energy pathway in the triplet state and the corresponding adiabatic and singlet potentials for a dissociation over the fcc site with the molecular axis aligned parallel to the surface in the geometry shown in the inlet. From Carbogno *et al.* [39].

be able to overcome the barrier on the "triplet" PES can dissociate in MQC due to a non-adiabatic spin-flip after reaching the triplet-singlet crossing seam. Not too surprisingly, this increase of the sticking coefficient observed in the MQC simulations is more pronounced for a larger electronic coupling. At high incident energies, the MD and the MQC approach again yield similar results, since the molecules are able to overcome the barrier regardless of the occurrence or absence of non-adiabatic transitions.

Certainly, these MQC simulations further substantiate that non-adiabatic spin-transitions are a possible explanation for the observed discrepancy between adiabatic theory and experiment. However, they also demonstrate that the initial sticking coefficient S_0 is not particularly sensitive to such non-adiabatic transitions, given that the shape of S_0 is largely determined by the barriers on the triplet PES alone. Along these lines, one might even speculate that the discrepancy found between the adiabatic simulations and the experiment is not related to non-adiabatic spin-transitions at all, but rather to shortcomings of the semi-local GGA exchange-correlation functional employed in the DFT calculations for the PES. In spite of the fact that a series of model studies for selected trajectories and/or finite aluminum clusters seem to support such speculations [46, 47, 48, 49], this nagging doubt is hard to settle in a rigorous fashion: On the one hand, studies of finite clusters and/or selected trajectories hardly allow to draw conclusions with respect to the full six-dimensional dynamics on the semi-infinite Al(111) surface; on the other hand, calculations with more advanced exchange-correlation functionals (or alternatively higher quantum chemical approaches) are at present computationally too involved for a mapping of the six-dimensional PES in extended supercell geometries, let alone that there is no clear candidate technique in sight that one would expect to give a fully quantitative description of both the localized O_2 electronic structure and the delocalized metal electrons.

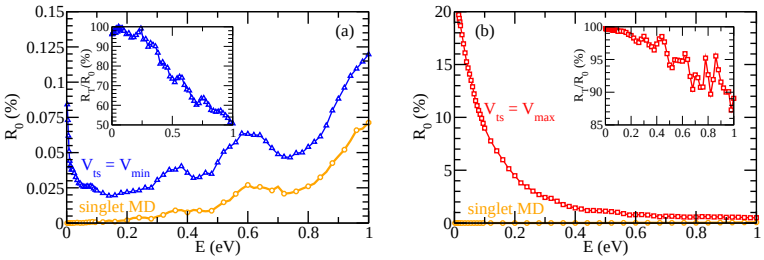

Fig. 4 Figs. (*a*) and (*b*) show the reflection coefficient R_0 as computed by MQC simulations for minimal and maximal coupling, respectively (see text). Additionally, the reflection coefficient produced by MD simulations solely on the singlet PES is shown as reference. In the insets, the respective relative yields of reflected triplet molecules R_T/R_0 are shown as well. From Carbogno *et al.* [40].

For this exact reason, Carbogno *et al.* proposed [39] to instead shift the focus to the scattering of singlet oxygen molecules from the Al(111) surface, for which they predicted unambiguous signatures for the occurrence of non-adiabatic spin-transitions. The idea behind this proposition is that such non-adiabatic effects can always be characterized by the conversion of electronic potential energy into nuclear kinetic energy (or vice versa). In the case of the regular triplet O_2 sticking coefficient, the kinetic energy gained due to the transition to the singlet state is, however, dissipated into the bulk and hence hardly accessible to precise experimental detection. This is not the case for the complementary process, i.e., the scattering of singlet oxygen molecules. As shown in Fig. 4, MQC simulations predict a notable amount of backscattered molecules for this process in spite of the fact that the singlet PES does not exhibit any barriers at all. Even more importantly, the vast majority of the reflected molecules are found in the spin-triplet state, since the interaction with the surface strongly favors the relaxation to the electronic ground state. At low incident energies, a notable fraction of trajectories undergoes such an electronic relaxation to the repulsive triplet PES already while approaching the crossing seam, which in turn leads to a tremendous increase of the reflection coefficient R_0. These non-adiabatic transitions go hand in hand with a conversion of electronic potential energy to nuclear kinetic energy, i.e., a characteristic heating of the vibrational and rotational degrees of freedom in scattering [39, 40]. Such molecular excitations are directly accessible to measurement. Thus performing the proposed experiment of scattering singlet oxygen molecules at Al(111) would allow to unambiguously determine the role of non-adiabatic spin-flips in the O_2/Al(111) interaction.

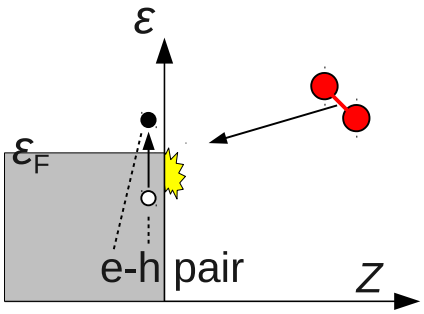

Fig. 5 Schematic illustration of electron-hole pair excitation during the impingement of a gas particle on a metal surface. An electron is excited from an occupied state below the Fermi level ε_F to an unoccupied state above, resulting in an excited state commonly referred to as electron-hole (e-h) pair.

3.2 Adsorption Dynamics of O_2 at Pd(100): Weak Electronic Non-Adiabaticity

As mentioned in the introduction the notion of a highly non-adiabatic dissociation dynamics in the O_2/Al(111) system was largely motivated by recalling that both generally discussed coupling mechanisms are largely suppressed: Spin-orbit coupling is still weak owing to the low mass number of Al [40], while the low Al density-of-states at the Fermi-level minimizes a tunneling of electrons between substrate and adsorbate. In this picture, it is instructive to contrast the O_2/Al(111) findings with a corresponding analysis of O_2 at Pd(100). Not only is the mass number of Pd significantly higher, thereby leading to stronger spin-orbit coupling. Moreover, with Pd in any case close to fulfilling the Stoner criterion for band ferromagnetism [50], Pd(100) is in particular the one surface orientation with highest density-of-state at the Fermi-level [51, 52, 53, 54]. This suggests the dissociation dynamics to be predominantly adiabatic, a perception that receives support by an excellent agreement of the computed adiabatic sticking coefficient with available experimental data [55].

Nevertheless, precisely the large number of states close to the Fermi level could also facilitate very efficient electron-hole pair excitations, cf. Fig. 5 - a view that has been repeatedly emphasized by Tully and others [44, 56, 57, 58, 59]. The role of such excitations in the adsorption dynamics might not be visible for a rather benign quantity like sticking or might even simply be hidden due to fortuitous error cancelation e.g. with the underlying DFT energetics. From the perspective of energy dissipation, however, they might be very important. As such, O_2 dissociation at Pd(100) is a most suitable model system to investigate such electronic non-adiabaticity due to substrate degrees of freedom. With a chemisorption energy computed as 2.6 eV at the DFT GGA-PBE level [60] the objective is thus to assess how much of this total amount is dissipated into electron-hole pairs. In turn, this would then provide indirect information on how relevant this channel is for the actual dissociation dynamics.

When screening possible approaches to provide such a (semi-quantitative) estimate, one unfortunately quickly realizes that the switch from the "fruit fly adsorbate", i.e. (atomic or molecular) hydrogen, to "another' diatomic" (as sketched in the introduction) is not a trivial step also with respect to available first-principles methodology [61]: The time-dependent Newns-Anderson model developed by Mizielinski and coworkers has never been applied to other adsorbates than (atomic) hydrogen [62, 63, 64, 65]. Even if parametrized based on DFT in the same way as in that work, it bears the risk of relying upon a too approximate description of the electronic structure for the semi-quantitative estimate desired here. Very accurate "direct" *ab initio* simulation of electron-hole pair excitations within time-dependent (TD-) DFT and Ehrenfest dynamics for the nuclei have also only been applied to hydrogen atoms impinging on the (111) surface of aluminum due to the even for this much simpler system almost intractable computational demands [66, 67, 68]. When therefore looking for more effective treatments, one has to recognize that approaches based on electronic friction theory [44, 69, 70, 71] depend critically on the way how friction coefficients are calculated. When relying on the local density friction approximation (LDFA), an application in six-dimensional dynamical studies of diatomics interacting with rigid surfaces is tractable [72], but has been criticized to not be sufficiently accurate [73, 74]. More accurate calculations of electronic friction coefficients are possible [75] and have proven very successful for the description of electronic damping of adsorbate vibrational motion [76]. Notwithstanding, they have never been used together with a high-dimensional adsorbate-substrate PES of *ab initio* quality so far [77, 78]. More severely, already first applications within a forced oscillator model (FOM) for the electrons of the substrate have revealed the proper description of spin transitions as an intrinsic shortcoming of electronic friction theory [79, 80]. This, of course, makes any method based on the latter highly problematic when trying to describe the adsorption dynamics of oxygen molecules.

In this situation, a new approach originally proposed by Timmer and Kratzer is highly appealing [81, 82]. It relies on perturbation theory applied to a TD-DFT framework. For any considered trajectory of an impinging molecule the essential idea is to approximate the real time-dependent effective potential by its counterparts in a series of snapshots of the respective separate non-time-dependent ground state problems. This motivates a Fermi's golden rule type expression for the transition probabilities, which yield spin-resolved excitation spectra when integrated along trajectories. The total amount of energy dissipated into electron-hole pair excitations is then obtained in a straight-forward fashion by energy weighted integrals over these spectra. Applying this approach to the O_2 interaction with Pd(100), Meyer and Reuter focused on four selected (non-dissociative) trajectories [60], obtained from a six-dimensional PES and chosen to span the range of possible impingements: Contrasted were side-on and head-on approaches over different high-symmetry sites of the Pd(100) substrate. Figure 6 compiles the corresponding results for one of these trajectories. As a first important insight, the energy loss and underlying e-h pair spectra differed considerably for the different impingements, with the absolute loss becoming larger the closer the molecule encounters the surface. This constitutes already a nice confirmation of one of the key results of the electron friction work

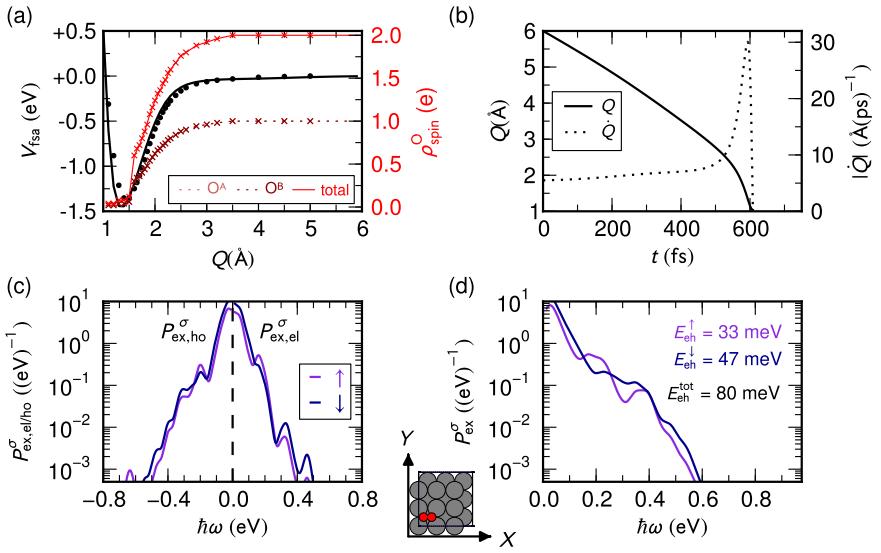

Fig. 6 Electron-hole pair excitations created by an O_2 molecule impinging side-on above a hollow site (*h-para*) as shown in the inset at the bottom. (a) PES V_{fsa} along the trajectory given by the reaction coordinate Q (neural network interpolation = black solid line, DFT input data = black circles), as well as projections of the spin density onto the two constituting oxygen atoms (O^A, O^B = dotted lines in shades of dark red, sum of O^A and O^B = light red solid line). (b) Evolution of reaction coordinate $Q(t)$ and corresponding velocity $\dot{Q}(t)$ with time t along the trajectory. (c) Separate electron (at positive excitation energies) and hole (at negative excitation energies $\hbar\omega$) spectra $P^\sigma_{ex,el}(\hbar\omega)$ and $P^\sigma_{ex,ho}(\hbar\omega)$. (d) Total e-h pair spectrum $P^\sigma_{ex}(\hbar\omega)$ together with resulting total dissipated energies. All spectra are for a half round trip with excitation energies $\hbar\omega$ relative to the Fermi energy. Both majority (↑, violet) and minority (↓, blue) spin channels are shown. From Meyer and Reuter [60].

of Juaristi *et al.* [72]: The importance of the high dimensionality of the molecule-substrate interaction also extends to e-h pair excitations. A proper assessment of the role of this dissipation channel thus needs to necessarily rely on a representative set of impingement scenarios and not just one model trajectory. Notwithstanding, even for the trajectory with the closest encounter to the surface, the total loss into e-h pair excitations only yields about 80 meV. Even when tripling the initial kinetic energy of the impinging molecule, this "educated maximum estimate" is not changed significantly. Consequently, the e-h pair excitation channel is unlike to dissipate more than 5% of the total chemisorption energy. On the one hand, this is very much in line with the findings of other studies going beyond single atoms at metal surfaces, regardless of whether the impinging diatomic molecule carried a permanent dipole moment (HCl on Al(111) [83]) or not (H_2 on Cu(110), N_2 on W(110) [72]), as well as with the hitherto unsuccessful attempts to detect chemicurrents in experiments over polycrystalline palladium [84]. On the other hand, it is remarkably low compared to e.g. H impingement over the threefold hollow site of Al(111). The latter leads to a comparable release of chemisorption energy as in the O_2/Pd(100) sys-

tem, but the computed amount of energy taken up by e-h pairs was one order of magnitude more, i.e. 1 eV (albeit likely favored by a penetration of the adsorbate into the first substrate layer) [66]. In this situation it is difficult to arrive at a final conclusion as to the relevance of electronic excitations in adsorption processes at metal surfaces in general. With recent quantitative sticking coefficient calculations for O_2/Ag(111) finding no necessity to invoke electronic non-adiabaticity to rationalize the measurements [85], it seems, however, that with respect to the sticking of O_2 noticeable effects are at best restricted to alkali, alkaline earth or simple metals. Indeed, for Mg(0001) and Al(111), a description of adsorption dynamics beyond the Born-Oppenheimer surface within the simple model of Hellman has provided good agreement with available experimental data [86, 87, 88].

4 Adiabatic dissociation dynamics and phononic dissipation

Even at surfaces, where electronic non-adiabaticity can be fully dismissed, life does not become any easier for the quantitative modeler aiming to study the O_2 dissociation dynamics. In comparison to e.g. the case of hydrogen at metal surfaces, the PES underlying the dissociation dynamics is governed by complex metal-O_2 π-orbital interactions and correspondingly much more structured. This leads to a large degree of complexity involving the co-existence of molecular and atomic adsorption states. Furthermore, the release of a rather sizable amount of chemisorption energy (typically of the order of several eVs) dictates to extend the description beyond the molecular degrees of freedom. Instead of a mere 6D PES, as customary in the traditional hydrogen dissociation studies, some account of heat dissipation into the substrate phonon bath needs thus to be included in the model. This complexity has to date only been met by a few seminal studies, and often using rather strong approximations. As this survey cannot provide an exhaustive account anyway, we will deliberately not cover more widespread qualitative approaches to include substrate motion in dynamical studies, as e.g. surface oscillators [89] or generalized Lagevin-type models [90]. Instead, the following selected showcases serve merely to illustrate the complexity and new physics encountered when moving to the ”more complex “diatomic”, as well as first attempts to describe heat dissipation more quantitatively.

4.1 Tight-binding molecular dynamics simulations of the O_2/Pt(111) adsorption dynamics

One of the first attempts to include a more quantitative treatment of phononic energy dissipation into the modeling of the dissociation process concerned the O_2/Pt(111) system. Due to its substantial technological relevance, e.g. with respect to car-exhaust catalysts [91] or for fuel cell electrodes [92], this system has been the ob-

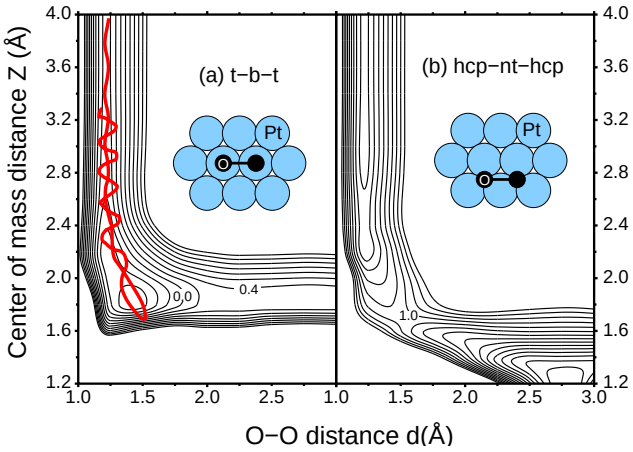

Fig. 7 Potential energy surface of the dissociation of O_2/Pt(111) determined by the *ab initio* derived tight-binding Hamiltonian. The coordinates in the figure are the O_2 center-of-mass distance from the surface Z and the O-O interatomic distance d. The configurations of the remaining O_2 degrees of freedom are illustrated in the insets. The contour spacing is 0.2 eV per O_2 molecule. In (a) a trajectory of an O_2 molecule with an initial kinetic energy of 0.6 eV scattered at Pt(111) is also plotted. From Eichler *et al.* [104].

jective of a significant number of studies [93, 94, 95, 96, 97, 98, 99, 100], rendering it among the best studied systems in surface science.

At surface temperatures below 100 K, three molecular O_2 adsorption states on Pt(111) have been identified. Below 30 K, a weakly bound physisorbed species exists [94]. Up to 100 K, two different kinds of molecularly chemisorbed states are found [101, 102] which have been characterized as peroxo-like (O_2^{-2}) and superoxo-like (O_2^{-}), respectively. This assignment of the chemisorbed molecular states has been confirmed by electronic structure calculations at the DFT-GGA level [103, 104]. According to these calculations, the superoxo-like O_2 species that still has a magnetic moment corresponds to an O_2 molecule adsorbed over the bridge position with the two O atoms oriented towards the adjacent Pt atoms in a so-called top-bridge-top (t-b-t) configuration, whereas the non-magnetic peroxo species has been identified as O_2 molecules adsorbed in a slightly tilted bridge-hollow-top configuration above the threefold hollow sites. Interestingly enough, molecular beam experiments yielded the rather surprising result that oxygen molecules do not dissociate at cold Pt surfaces below 100 K [95, 98, 99], even at the highest accessible kinetic energies of 1.4 eV which are much higher than the dissociation barrier.

The PES of O_2/Pt(111) derived from DFT-PBE calculations [104] is illustrated in Fig. 7 where two representative elbow plots are shown. They correspond to two-dimensional cuts of the PES as a function of the O_2 center-of-mass distance from the surface and the O-O interatomic distance. Panel (a) presents the elbow plot of the superoxo molecular precursor state located above the bridge site. The access

from the gas phase is non-activated, i.e. it is not hindered by any barrier. The peroxo states above the threefold hollow sites (not shown) which are energetically almost degenerate with the superoxo state [103] can also be directly accessed from the gas phase. Note that there is a large uncertainty with respect to the choice of the GGA functional, as far as the O_2-Pt(111) interaction is concerned. Using the GGA-PBE functional [8] the adsorption energy in the superoxo state is -0.6 eV [104] whereas it is reduced to -0.1 eV [100] when the GGA-RPBE functional [10] is used.

As Fig. 7 demonstrates, the interaction of O_2 with Pt(111) crucially depends on the lateral position of the O_2 molecule, i.e. the O_2/Pt(111) PES is strongly corrugated. By shifting the molecule by about 1 Å in lateral direction from the superoxo configuration to a near-top site, the nature of the interaction is changed from attraction towards the molecular precursor (Fig. 7b) to strong repulsion with a barrier towards dissociation of almost 1 eV (Fig. 7b), which is further increased to 1.3 eV for O_2 above the top position [104]. In addition, the PES is highly anisotropic, molecules approaching the surface in an upright fashion experience pure repulsion. Also rotations with the O_2 axis parallel to the surface are strongly hindered for example at the threefold hollow positions [104]. In fact, the majority of adsorption channels are hindered by barriers; direct non-activated access of the molecular precursor states is possible for only a small fraction of initial conditions.

In molecular, i.e. non-dissociative adsorption, the impinging molecule can only stay at the surface if it transfers its excess kinetic energy to the substrate degrees of freedom. This means that in order to reliably determine sticking probabilities of O_2 on Pt(111), an accurate representation of the PES has to be coupled with an appropriate modeling of surface recoil and energy dissipation. This requires to take into account a rather large number of degrees of freedom in the simulations. To date this can only been done in classical simulations since the computational effort in quantum dynamical simulations rises exponentially with the considered degrees of freedom. In order to avoid the large cost of direct *ab initio* molecular dynamics (AIMD) simulations, the first dynamical studies of the adsorption of O_2 on Pt(111) were performed using a tight-binding molecular dynamics (TBMD) scheme [105] with the O-Pt interaction parameter derived from DFT calculations, describing the adsorption in a periodic setup within a $c(4\times4)$ unit cell.

The sticking probabilities of O_2/Pt(111) derived from the TBMD simulations [106, 107] are compared with the experiment in Fig. 8a. Although still quantitative discrepancies between theory and experiment exist, the agreement is satisfactory. More importantly, the TBMD simulations helped to clarify important dynamical aspects of the O_2/Pt(111) interaction. The experimentally observed initial strong decrease of the sticking probability as a function of the kinetic energy was originally associated with the trapping into a molecular physisorption state [98, 99]. However, the potential energy surface on which the TBMD simulations were based on did not exhibit any physisorption well. Instead, the strong decrease of the sticking probability is caused by the strong suppression of steering [108] to the molecular chemisorption well. Thus it is not the energy transfer *per se* that determines the trapping probability as usual in molecular adsorption, but rather the probability to enter the molecular chemisorption state.

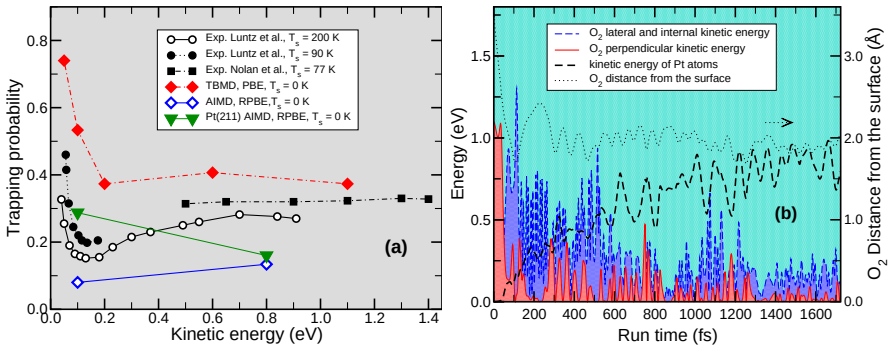

Fig. 8 Panel a: Trapping probability of O_2/Pt(111) as a function of the kinetic energy for normal incidence. Results of molecular beam experiments for surface temperatures of 90 K and 200 K (Luntz *et al.* [93]) and 77 K (Nolan *et al.* [99]) are compared to tight-binding molecular dynamics simulations [106, 107] for the surface initially at rest ($T_s = 0$ K) and AIMD simulations for O_2 on Pt(111) and Pt(211). Panel b: Energy redistribution in eV and O_2-Pt(111) distance in Å along a TBMD trajectory for an initial kinetic energy of $E_{kin} = 1.1$ eV. From Gross *et al.* [106].

The TBMD simulations also reproduced the experimental findings that the impinging O_2 molecules do not directly dissociate, even at the highest kinetic energies that are much larger than the dissociation barrier. This observation can be explained by the PES topology. In Fig. 7a, the projection of a trajectory approaching the superoxo chemisorption state is shown; the initial energy of the O_2 molecule was 0.6 eV. This energy is sufficient to enter the channel towards dissociative adsorption. Yet, the molecule is first accelerated towards the chemisorption well and then scattered at the repulsive wall of the potential. Entering the dissociation channel requires a conversion of the energy perpendicular to the surface into the O-O vibrational mode, but the curvature of the PES does not induce such a conversion. This does not mean that direct dissociative adsorption of O_2 on Pt(111) is not possible, it is just very unlikely. Hence the dissociation of O_2 on Pt(111) is typically a two-step process: First the molecule becomes trapped in a chemisorption well, and then induced by thermal fluctuation it might enter the dissociation channel.

Another experimental fact is reproduced by the TBMD simulations, namely the leveling off of the sticking probability at high kinetic energies. This behavior is surprising since in atomic and molecular adsorption the sticking probability typically decreases monotonically with increasing kinetic energy, since the energy transfer necessary for sticking becomes less efficient at higher kinetic energies [109]. In fact, if the impinging O_2 molecule is treated as a point-like object, it would never stick at the surface at such high energies [106, 107]. Hence it is important to take all relevant degrees of freedom into account in order to understand the sticking process. In Fig. 8b, the energy redistribution of a O_2 molecule hitting the Pt(111) surface along a TBMD trajectory leading to sticking for an initial kinetic energy of $E_{kin} = 1.1$ eV is plotted. Directly after the first impact, most of the initial kinetic energy of the molecule is transferred into internal degrees of freedom (rotations and vibrations) and kinetic energy lateral to the surface. This energy is not available for escaping

the surface again. Consequently, the O_2 molecule becomes dynamically trapped. In this trapped state, it continues to bounce back and forth with respect to the surface, and with each bounce it transfers an additional amount of energy to the surface that is taken up by surface vibrations. Eventually, after 1.5 ps, most of the initial energy is transferred to the substrate, i.e. the molecule has equilibrated with the surface, and the molecule's energy is not sufficient any more to leave the surface.

There is, however, one technical problem with these simulations. The TBMD simulations have been performed within the microcanonical ensemble which means that the total energy of the systems is kept constant along the trajectory. Consequently, during the dissociative sticking a large fraction of the initial kinetic energy plus the chemisorption energy has to be taken up by the substrate vibrations. As Fig. 8b demonstrates, the Pt substrate atoms have in fact gained about 1 eV kinetic energy upon the adsorption of the O_2 molecule. In principle this energy should be dissipated into the Pt bulk via phonon propagation and anharmonic phonon decay. However, because of the finite unit cell, this is not possible. The created phonons are literally reflected by the periodic boundary conditions. This leads to a spurious strong local heating of the surface. For the assessment of the initial molecular trapping and dissociation, this should not be too much of a problem. Following the longer-term adsorbate motion ensuing the dissociation process (possibly until the full equilibration with the substrate) is, however, impossible without including some form of extended phononic heat bath into the modeling.

4.2 Ab initio molecular dynamics simulations of the O_2/Pt(111) and O_2/Pt(211) adsorption dynamics

Due to the implementation of more efficient algorithms and the ever-increasing computer power it has recently become possible to perform a statistically sufficient number of *ab initio* molecular dynamics (AIMD) simulations of adsorption processes at metal surfaces [110] in which the forces necessary to integrate the equations of motions are determined "on the fly" by first-principles electronic structure calculations. In Fig. 8a, preliminary results of AIMD simulations of O_2/Pt(111) are included. The obtained trapping probabilities are somewhat smaller that those derived from the earlier TBMD simulations. This can be related to the fact that the RPBE functional [10] has been employed in the AIMD simulations which leads to a more repulsive O_2-Pt(111) interaction than within the PBE functional [9] that was used to derive the tight-binding Hamiltonian.

The agreement is nevertheless good enough to demonstrate that AIMD simulations can nowadays yield similar quality results as preceding divide-and-conquer approaches based on interpolated PESs (at least for near-unity sticking coefficients where statistics are rather benign). This is good news in the sense that AIMD simulations offer a much more straightforward way to include substrate mobility, and thus phononic heat dissipation. The computational effort of AIMD is furthermore basically related to the size of the unit cell so that also more complex surface struc-

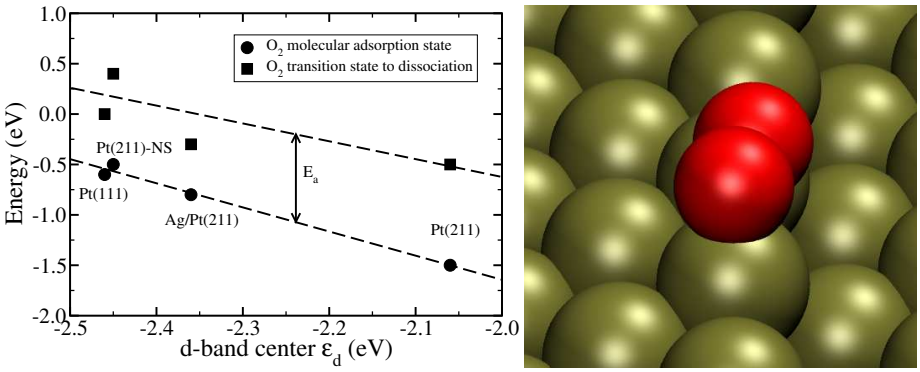

Fig. 9 Left panel: Calculated molecular O_2 adsorption energies and energies of the transition state towards dissociative adsorption as a function of the local d-band center ε_d [100, 112]. Right panel: Snapshot at $t = 6.3$ ps of an AIMD trajectory of O_2 impinging on Pt(211).

tures can be accessed as long as the unit cell does not become too large. Considering the above mentioned restrictions with respect to the reliability of longer-time evolution (unless enabling additional heat bath dissipation as explained in Section 4.3 below), microkinetic AIMD simulations are thus particularly suited to study the initial adsorption dynamics on e.g. precovered [110, 111] or stepped surfaces.

Scanning tunneling microscopy experiments have revealed that O_2 molecules preferentially dissociate at step sites of vicinal Pt surfaces [100]. Corresponding DFT calculations have shown that the O_2 dissociation barriers are in fact slightly larger at the steps than on terraces (see Fig. 9) [100, 112] which seems to be at variance with the experimental findings. However, the O_2 binding to the steps is much stronger than to the terraces so that molecules approaching the steps gain a much higher energy. Still, the consequences of this much higher energy gain upon adsorption on the dissociation dynamics have been unclear.

In order to clarify this issue, AIMD simulations of O_2 impinging on Pt(211) have been performed. Figure 8a also includes estimated sticking probabilities derived from these simulations for two different initial kinetic energies $E_{\mathrm{kin}} = 100$ and 800 meV. As expected, because of the higher adsorption energy, these sticking probabilities are larger than those derived from the AIMD simulations for the flat Pt(111) surface. Interestingly enough, the much higher adsorption energy on Pt(211) apparently only plays an important role at low kinetic energies. Surprisingly, at high kinetic energies the sticking probabilities on Pt(111) and Pt(211) are rather similar. This is most probably due to the fact that the sticking probability is largely determined by the trapping into the dynamical precursor which does not depend significantly on the well depth.

An analysis of the trajectories leading to sticking reveals that the O_2 molecules in these cases all end up at the energetically most favorable site at the upper side of the steps. The right panel of Fig. 9 shows the final state of an O_2 molecule initially impinging on the terrace of the Pt(211) surface. Apparently the mobility of the O_2 molecules after being trapped is still high enough that they all find the en-

ergetically most favorable adsorption site before they become fully accommodated. This supports the experimental observation of preferential oxygen adsorption at the steps.

4.3 Hot-adatom motion: O_2 dissociation at Pd(100)

Either through TBMD or AIMD the work reviewed in the preceding two sections has allowed for a first treatment of substrate mobility. In contrast to earlier divide-and-conquer approaches (at best coupled to qualitative surface oscillator models) this enables a much more realistic simulation of initial trapping probabilities or even molecular dissociation out of trapped states. Due to the microcanonic setup in periodic supercell geometries, there are, however, still two fundamental shortcomings inherent to these approaches: Even in the largest supercells, which are currently at the limit of being computationally tractable within AIMD simulations, substrate phonons with small wave lengths are still not well described. Even worse, surface phonons, which are often assumed to be crucial for the energy uptake in simple models [113], are not described at all as a sufficiently large number of slab layers cannot be afforded in those state-of-the-art simulations. Second, the propagation of any excited phonon mode is limited due to the unphysical reflections at the supercell boundaries, i.e. the energy transferred into the phononic degrees of freedom has no possibility to leave the system. This can lead to a significant unrealistic heating of the substrate in the simulations, with concomitant consequences for the (longer-term) adsorbate dynamics. Therefore, it is not surprising that a proper account of substrate mobility has only recently been termed as one of the present key challenges for the theoretical modeling in molecule-surface reactions for any molecule heavier than H_2 [114].

There are a number of approaches in the literature that could provide such a heat sink for molecular dynamics simulations of surface processes, thus accounting for energy dissipation. Within the spirit of an Einstein phonon model, one of the simplest ones would be the already mentioned qualitative surface oscillator models [89, 115, 116]. While only recently an attempt was made to estimate the few material specific parameters of the former by evaluating couplings to individual surface atoms [117], very often surface phonon modes have been used [113]. Quite in contrast, a potentially large but ”only” harmonic bath representing the vibrational degrees of the substrate can be included when constructing system-bath model Hamiltonians of Lindblad form in the context of gas-surface dynamics – originally motivated by a quantum mechanical treatment of the nuclei in case of hydrogen adsorbates [118, 119]. Notwithstanding, in practice, state-of-the-art versions of these Hamiltonians are still based on parametrized model potentials for the system and system bath interactions [120]. Going beyond linear system-bath coupling and thus from one-phonon to multi-phonon processes [121, 122, 123, 124, 120] represents a hitherto largely unsolved challenge [125]. Another numerically undemanding and at first glance intuitive approach to withdraw energy from the finite

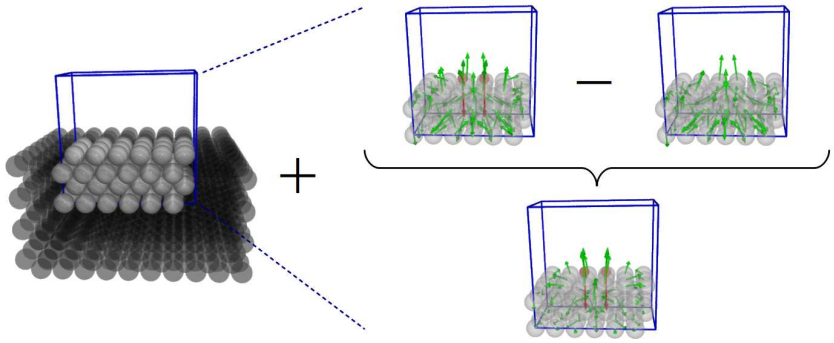

Fig. 10 Schematic illustration of the QM/Me scheme for metallic systems: A periodic simulation cell (blue) treated within DFT (QM), thus allowing for an accurate description of the metallic band structure and its implications for the adsorbate-substrate binding, is embedded into a large bath treated at the MEAM (MM) level as shown on the left: Only the adsorbate and adsorbate-substrate interaction are extracted from the former by forming differences between the former with and without adsorbate (right, upper part). Following the nearsightedness principle, resulting differences of Hellman-Feynman forces (green) decay quickly with increasing distance from the adsorbate (right, bottom) and can thus be embedded.

supercell would be to employ thermostats that yield continuous trajectories (e.g. [126]). In this widespread molecular dynamics concept the equations of motion are modified in such a way that an appropriate ensemble of trajectories provides correct non-*NVE* statistical properties. Within a canonical ensemble description thermostats would therefore by construction withdraw the released adsorption energy to maintain a preset system temperature. However, thermostats are in general only designed as a sampling tool to obtain correct statistical properties of the system at equilibrium. *A priori*, it is highly questionable whether the rate with which they withdraw the released excess energy during the non-equilibrium process given by an adsorption event is properly described. In addition, in this statistical approach the individual trajectories lose their physical meaning, thereby giving away much of the important dynamical information specifically sought in AIMD of adsorption processes. This disadvantage applies equally to the family of approaches relying on generalized Langevin equations (e.g. [90]), which furthermore also treat the substrate as a harmonic solid. In addition, just like the model Hamiltonians mentioned before, these approaches rely on the Markov approximation when integrating out bath degrees of freedom [90, 118, 123] – assuming that the phononic system of the substrate is only weakly perturbed from equilibrium. This might be problematic if most of the dissipated energy is at least initially deposited into a small set of modes (e.g. predominantly surface modes).

A deterministic approach, which should allow to investigate most of the aforementioned assumptions from a first-principles point of view, would instead be the well-known QM/MM ansatz: A small quantum-mechanical region is embedded into

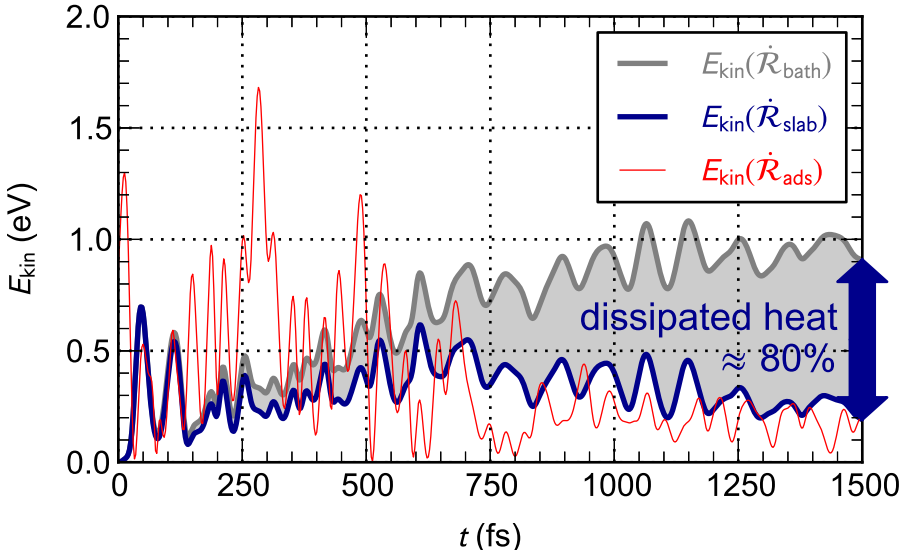

Fig. 11 Heat dissipation during O_2 dissociation at Pd(100): Total kinetic energy of all palladium atoms in the bath (thick gray line) as well as those in the QM/Me embedding cell contained therein (thick blue line) as a function of time. The area between these two curves is a measure for the dissipated heat. In addition, the kinetic energy of the dissociating oxygen molecule is also shown (thin red line). From Meyer and Reuter [129].

a very large environment described at the molecular-mechanics level [127]. The latter, for metallic substrates e.g. a modified embedded atom method (MEAM) potential [128], is computationally much less demanding compared to electronic structure calculations. The MM region could therefore easily be chosen large enough to effectively mimic energy dissipation into the bulk on the time scales relevant for the adsorbate equilibration. The problem that prevents the direct applicability of this ansatz to metallic systems is that the latter are necessarily described within periodic boundary condition calculations to accurately represent the metallic band structure [127]. This dilemma has recently been overcome by Meyer and Reuter with an approach coined ”QM/Me” [129]. The essential idea of the approach is to separate chemical and elastic contributions to the substrate forces arising during a dissociative adsorption process. Treating the short-ranged chemical forces at the DFT level, and the long-ranged elastic contributions at the MEAM-level, cf. Fig. 10, corresponding QM/Me dynamical simulations allow to seamlessly enrich AIMD at metal surfaces by a quantitative account of the physics of (surface) phonons.

A first application of this novel ansatz has focused on the dissociation dynamics of O_2 at Pd(100). The work built on a preceding detailed analysis of the PES at larger distances from the surface (obtained in the traditional divide-and-conquer way for a static Pd(100) substrate, cf. section 3.2), which identified a strong steering of almost all impinging molecules into one dominant entrance channel [55]. The QM/Me simulations correspondingly focused on a representative trajectory initiated

in this entrance channel. The results summarized in Fig. 11 provide a direct confirmation of the relevance of the QM/Me-embedding, i.e. to include an extended heat bath to properly describe the dynamics of a surface process as exothermic as the dissociation of oxygen. The essential adsorbate dynamics until near equilibration with the substrate takes roughly place in a time span of 1.5 ps, at which moment the remaining kinetic energy on each O atom is still somewhat above 75 meV. The rest of the sizable 2.6 eV chemisorption energy, cf. section 3.2, has gone into substrate degrees of freedom, and, most importantly, 80% of this released heat has already left the DFT surface unit-cell. In any conventional microcanonic AIMD simulation this substantial amount of heat would have been spuriously reflected by the periodic boundary conditions and then led to a falsification of the adsorbate motion.

While this underscores the importance of the energy transfer to the substrate, the results in turn also show that even after 1.5 ps still some of the released chemisorption energy is left in the molecular degrees of freedom. The transfer is thus nowhere near "instantaneous", which in fact shows up dramatically in the adsorbate motion ensuing the actual dissociation event. As shown in Fig. 11 the released chemisorption energy first leads to a steep increase of the oxygen kinetic energy. This creates "hot" adatoms that rapidly slide over several lattice constants while successively losing their kinetic energy to phonon excitations. Within the recorded 1.5 ps the adatoms thus travel over four bridge-site transition states. This "hot" diffusive motion would have taken on the order of milliseconds in thermal equilibrium at room temperature according to conventional transition state theory and the computed static DFT-PBE barrier. A corresponding "hot adatom" motion after dissociative adsorption has recently been found in AIMD simulations of the dissociative adsorption of H_2 on Pd(100) [130] and has been repeatedly inferred from experiments addressing O_2 dissociative adsorption, prominently at Al(111) [31, 131] or Ag(100) [132], but could never be confirmed by theoretical modeling before for O_2/metal systems [133, 134].

One possible reason for this discrepancy could be that preceding modeling analyzed this phenomenon from too static a PES point of view, e.g. merely comparing the released chemisorption energy to the static diffusion barriers. One intriguing aspect that comes out of the seminal QM/Me-simulations at Pd(100) is instead a much more dynamic picture [136]: As shown for a snapshot along the computed trajectory in Fig. 12, the phonon excitations concentrate largely in one mode, namely the so-called S6 surface phonon mode [135]. This is a lateral mode that induces a kind of breathing motion of the top-layer Pd atoms perpendicular to the hollow-bridge-hollow [100] direction at the surface. This makes it intuitively plausible why preferentially this mode gets excited by a O adatom diffusing along hollow-bridge-hollow. Vice versa, however, the resulting strongly non-thermal population of this mode (and the corresponding strong lateral displacements of the Pd surface atoms surrounding the adatom) also couples back onto the diffusive motion: The Pd atoms literally make way for the approaching adatom, reducing the energetic barrier and fostering the hot translation into the next hollow site PES minimum [136].

Apart from these intriguing insights into the coupling between energy dissipation and adsorbate dynamics, the prominent population of the S6 mode also nicely

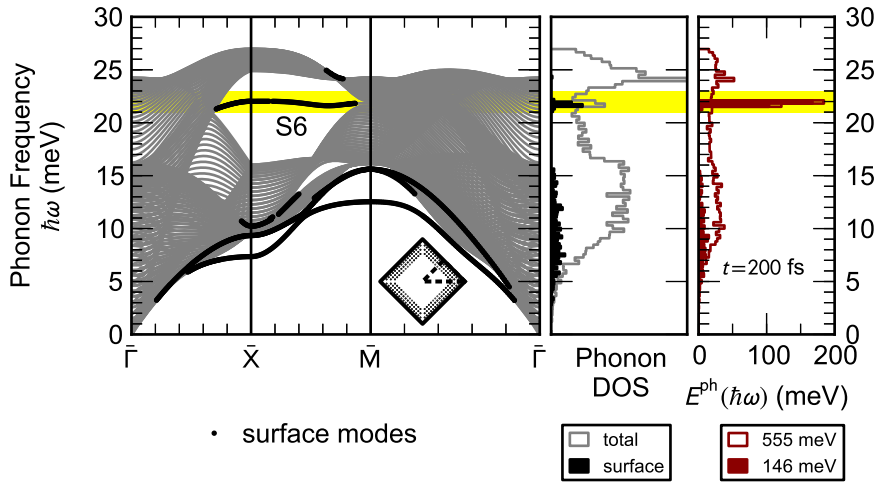

Fig. 12 Analysis of phonon mode excitation at $t = 200$ fs during the O_2 dissociation at Pd(100) trajectory summarized in Fig. 11. Surface-projected phonon band structure (left) and phonon density of states (right) are shown together with the actual population of modes $E^{\mathrm{ph}}(\hbar\omega)$ at this moment in time. A strongly non-thermal population of the so-called S6 surface phonon mode [135] can be discerned. From Meyer and Reuter [136].

reflects back on the level of modeling required to adequately treat the dissociation process. First of all, it is not the energetically low-lying Rayleigh modes that become dominantly excited – quite in contrast to what has been frequently assumed in model Hamiltonian studies [137, 121, 118, 123, 138, 139]. In contrast to the S6 mode these modes predominantly involve surface Pd atom displacements normal to the surface. Apart from the low energy cost to excite them, this displacement pattern has been one motivation for their consideration, viewing the adsorption impingement as leading to some form of surface indentation. Along these lines, the now revealed strong excitation of the S6 mode can thus be rationalized as a consequence of the adsorbate atom's ability to resolve the atomic structure of the surface: Rather than normally indenting a structureless substrate top layer, the dissociating O atoms move into the Pd(100) hollow sites and instead push the top layer atoms laterally aside. Second, the strong concentration on the S6 mode leads to a strongly non-thermal excitation of the latter, with about 100 meV stored in it for instance in the snapshot shown in Fig. 12. As mentioned above, such a multi-phonon nature of the excitation is difficult to grasp in common system-bath Hamiltonian approaches [125]. Moreover, with such a strongly non-thermal population also an appropriate description of phonon decay through anharmonicities in the substrate potential becomes relevant, otherwise the energy stored in the S6 mode is artificially kept close to the surface and may potentially affect the continuing adsorbate motion. Also this aspect is not commonly met in system-bath approaches, underscoring the relevance

of an accurate reference technique like QM/Me in identifying crucial aspects that need to be captured in simplified stochastic models.

5 Conclusions and Outlook

In this chapter we have reviewed recent progress in the modeling of the O_2 adsorption dynamics at metal surfaces. This modeling builds on an extensive body of work and insight obtained over the last 20 or so years for the H_2-metal interaction, previously considered as *the* prototype system for gas-surface dynamics. While the move from one diatomic to another might seem marginal at first glance, our discussion has highlighted a number of significant additional complexities not met in the preceding H_2-centered work. Some of these complexities could be mere specificities of the oxygen molecule. Others could as well be important general features found for any heavier adsorbate. The spin selection rule problematics in the O_2-metal interaction certainly belongs more to the prior category. On the other hand, as has become clear from the discussion, there is as yet no trend understanding as to the relevance of electronic non-adiabaticity during adsorption processes at metal surfaces at all, so the specific viewpoint from a spin-triplet gas-phase molecule might be quite helpful. What is for sure an important general feature not encountered in the prototype H_2/metal system is the necessity to accurately describe the dissipation of the released chemisorption energy, and therewith to account for substrate mobility in the modeling. This is already a crucial aspect in the typically rather exothermic O_2-metal interaction, and will become even more important when moving to even heavier/multi-atom adsorbate molecules.

Already by itself an appropriate modeling of energy dissipation in adsorption dynamics would be a severe methodological challenge. The necessity to account for it when moving away from the simple H_2/metal example, is, however, also accompanied by the necessity to adequately capture an increasingly complex and corrugated PES landscape, owing in the O_2 case to the interaction with the molecular π-orbitals. For multi-atom adsorbates the lowered symmetry and preferential interactions with different molecular moieties will further add to this complexity. Altogether this puts ever more emphasis on the need for sufficient statistical explorations and evaluations of the high-dimensional PESs. This higher dimensionality of adsorption processes of larger molecules at mobile substrates (compared to the situation for simple diatomics at static surfaces) might dictate a methodological shift away from prevalent divide-and-conquer approaches. On the other hand, it is precisely the need for sufficient statistics that would speak against their replacement by direct AIMD-type simulations (suitably augmented by some form of phononic heat bath) – at least for the time being. Solving this dilemma will be a central cornerstone of future work in this field. Most certainly it will require the advancement of existing and development of new theoretical machinery. Looking in retrospect at corresponding developments first undertaken for the H_2 adsorption dynamics and then for the here reviewed O_2 adsorption dynamics at metal surfaces, this is not a threat though. In the end it is

precisely this possibility to sharpen the methodological tools that makes work on the dynamics of such simple, yet well-defined model systems so worthwhile.

Acknowledgments

It is a pleasure to thank all colleagues who have contributed to the studies presented in this contributions, among others Jörg Behler, Sönke Lorenz, Christian Mosch, Michael Mehl, Dimitrios Papaconstantopoulos, and Matthias Scheffler. Furthermore, stimulating discussions with Maite Alducin, Iñaki Juaristi as well as Matthias Timmer and Peter Kratzer during various conferences and visits are gratefully acknowledged.

References

1. N. Cabrera, N.F. Mott, Rep. Prog. Phys. **12**, 163 (1949)
2. E. Wigner, Nachr. Ges. Wiss. Goett., Math.-Phys. Kl. p. 375 (1927)
3. F. Hund, Z. Phys. **33**, 345 (1925)
4. C. Schweitzer, R. Schmidt, Chem. Rev. **103**, 1685 (2003)
5. R.G. Parr, W. Yang, *Density-Functional Theory of Atoms and Molecules* (Oxford Science Publications, 1989)
6. N.H.F. Beebe, E.W. Thulstrup, A. Andersen, J. Chem. Phys. **64**, 2080 (1976)
7. D.M. Ceperly, B.J. Alder, Phys. Rev. Lett. **45**, 566 (1980)
8. J.P. Perdew, J.A. Chevary, S.H. Vosko, K.A. Jackson, M.R. Pederson, D.J. Singh, C. Fiolhais, Phys. Rev. B **46**, 6671 (1992)
9. J.P. Perdew, K. Burke, M. Ernzerhof, Phys. Rev. Lett. **77**, 3865 (1996)
10. B. Hammer, L.B. Hansen, J. Nørskov, Phys. Rev. B **59**, 7413 (1999)
11. G. Herzberg, *Molecular Spectra and Molecular Structure, I. Spectra of Diatomic Molecules* (van Nostrand Reinhold Company, New York, 1950)
12. R.C. Weast (ed.), *CRC Handbook of Chemistry and Physics (67th ed.)* (CRC Press, 1987)
13. P. Krupenie, J. Phys. Chem. Ref. Data **1**, 423 (1972)
14. C. Carbogno, Non-Adiabatic Effects in the Dissociative Adsorption of O_2 on Aluminum (111) Surfaces. Ph.D. thesis (2009)
15. F. Jensen, *Introduction to Computational Chemistry* (Wiley, 2002)
16. H. Partridge, J. C. W. Bauschlicher, S.R. Langhoff, P.R. Taylor, J. Chem. Phys. **95**, 8292 (1991)
17. E. Engel, S.H. Vosko, Phys. Rev. A **47**, 2800 (1993)
18. Y. Zhang, W. Yang, Phys. Rev. Lett. **80**, 890 (1998)
19. E.H. Lieb, S. Oxford, Int. J. Quantum Chem. **19**, 427 (1981)
20. R.K. Nesbet, Phys. Rev. A **56**, 2665 (1997)
21. J.R. Schmidt, N. Shenvi, J.C. Tully, J. Chem. Phys. **129**, 114110 (2008)
22. K.J. Ritter, T.D. Wilkerson, J. Mol. Spectrosc. **121**, 1 (1987)
23. M. Kasha, in *Singlet Oxygen*, ed. by A.A. Frimer (CRC Press: Boca Raton, 1985), p. 1
24. A. Berning, M. Schweizer, H.J. Werner, P.J. Knowles, P. Palmieri, Mol. Phys. **98**, 1823 (2000)
25. O. Spalek, J. Kodymova, P. Stopka, I. Micek, J. Phys. B: At., Mol., Opt. Phys. **32**, 1885 (1999)
26. R. Klotz, C.M. Marian, S.D. Peyerimhoff, B.A. Hess, R.J. Buenker, Chem. Phys. **89**, 223 (1984)

27. B. Minaev, O. Vahtras, H. Ågren, Chem. Phys. **208**, 299 (1996)
28. R.M. Badger, A.C. Wright, R.F. Whitlock, J. Chem. Phys. **43**, 4345 (1965)
29. B.F. Minaev, H. Ågren, J. Chem. Soc., Faraday Trans. **93**, 2231 (1997)
30. L. Österlund, I. Zorić, B. Kasemo, Phys. Rev. B **55**, 15452 (1997)
31. H. Brune, J. Wintterlin, R.J. Behm, G. Ertl, Phys. Rev. Lett. **68**, 624 (1992)
32. M. Schmid, G. Leonardelli, R. Tscheließnig, A. Biedermann, P. Varga, Surf. Sci. **478**, L355 (2001)
33. P.O. Gartland, Surf. Sci. **62**, 183 (1977)
34. A. Groß, *Theoretical Surface Science* (Springer, 2003)
35. Y. Yourdshahyan, B. Razaznejad, B.I. Lundqvist, Phys. Rev. B **65**, 75416 (2002)
36. J. Behler, B. Delley, K. Reuter, M. Scheffler, Phys. Rev. B **75**, 115409 (2007)
37. J. Behler, B. Delley, S. Lorenz, K. Reuter, M. Scheffler, Phys. Rev. Lett. **94**, 036104 (2005)
38. J. Behler, K. Reuter, M. Scheffler, Phys. Rev. B **77**, 115421 (2008)
39. C. Carbogno, J. Behler, A. Groß, K. Reuter, Phys. Rev. Lett. **101**, 096104 (2008)
40. C. Carbogno, J. Behler, K. Reuter, A. Groß, Phys. Rev. B **81**, 035410 (2010)
41. J.C. Tully, J. Chem. Phys **93**, 1061 (1990)
42. C. Bach, A. Groß, J. Chem. Phys. **114**, 6396 (2001)
43. C. Bach, T. Klüner, A. Groß, Appl. Phys. A **78**, 231 (2004)
44. M. Head-Gordon, J.C. Tully, J. Chem. Phys. **103**, 10137 (1995)
45. J.C. Tully, Faraday Discussions **110**, 407 (1998)
46. X. Fan, W. Lau, Z. Liu, Phys. Rev. Lett. **96**, 079801 (2006)
47. C. Mosch, C. Koukounas, N. Bacalis, A. Metropoulos, A. Groß, A. Mavridis, J. Phys. Chem. C **112**, 6924 (2008)
48. E. Livshits, R. Baer, R. Kosloff, J. Phys. Chem. A **113**, 7521 (2009)
49. H. Liu, H. Xiang, X. Gong, J Chem Phys **135**, 214702 (2011)
50. N.W. Ashcroft, N.D. Mermin, *Solid State Physics*, 1st edn. (Brooks Cole, 1976)
51. F.J. Arlinghaus, J.G. Gay, J.R. Smith, Phys. Rev. B **23**, 5152 (1981)
52. G.S. Elliott, K.E. Smith, S.D. Kevan, Phys. Rev. B **43**, 3893 (1991)
53. S.C. Wu, D.M. Poirier, M.B. Jost, J.H. Weaver, Phys. Rev. B **45**, 8709 (1992)
54. M. Heinrichsmeier, A. Fleszar, W. Hanke, A.G. Eguiluz, Phys. Rev. B **57**, 14974 (1998)
55. J. Meyer, K. Reuter, *First-principles Initial Sticking of O_2 at Pd(100)*, to be published (2012)
56. M. Head-Gordon, J.C. Tully, J. Chem. Phys. **96**, 3939 (1992)
57. A.M. Wodtke, J.C. Tully, D.J. Auerbach, Int. Rev. Phys. Chem. **23**, 513 (2004)
58. X. Li, J.C. Tully, H.B. Schlegel, M.J. Frisch, J. Chem. Phys. **123**, 084106 (2005)
59. N. Shenvi, S. Roy, J.C. Tully, Science **326**, 829 (2009)
60. J. Meyer, K. Reuter, New J. Phys. **13**, 085010 (2011)
61. B.I. Lundqvist, A. Hellman, I. Zorić, in *Dynamics*, *Handbook of Surface Science*, vol. 3, ed. by E. Hasselbrink, B. Lundqvist (North-Holland, 2008), pp. 429 – 524
62. M.S. Mizielinski, D.M. Bird, M. Persson, S. Holloway, J. Chem. Phys. **122**, 084710 (2005)
63. M.S. Mizielinski, D.M. Bird, M. Persson, S. Holloway, J. Chem. Phys. **126**, 034705 (2007)
64. M.S. Mizielinski, D.M. Bird, M. Persson, S. Holloway, J. Chem. Phys. **126**, 229901 (2007)
65. M.S. Mizielinski, D.M. Bird, M. Persson, S. Holloway, Surf. Sci. **602**, 2617 (2008)
66. M. Lindenblatt, J. van Heys, E. Pehlke, Surf. Sci. **600**, 3624 (2006)
67. M. Lindenblatt, E. Pehlke, Surf. Sci. **600**, 5068 (2006)
68. M. Lindenblatt, E. Pehlke, Phys. Rev. Lett. **97**, 216101 (2006)
69. E.G. d'Agliano, P. Kumar, W. Schaich, H. Suhl, Phys. Rev. B **11**, 2122 (1975)
70. M. Persson, B. Hellsing, Phys. Rev. Lett. **49**, 662 (1982)
71. B. Hellsing, M. Persson, Phys. Scr. **29**, 360 (1984)
72. J.I. Juaristi, M. Alducin, R. Dìez Muiño, H.F. Busnengo, A. Salin, Phys. Rev. Lett. **100**, 116102 (2008)
73. A.C. Luntz, I. Makkonen, M. Persson, S. Holloway, D.M. Bird, M.S. Mizielinski, Phys. Rev. Lett. **102**, 109601 (2009)
74. J.I. Juaristi, M. Alducin, R. Dìez Muiño, H.F. Busnengo, A. Salin, Phys. Rev. Lett. **102**, 109602 (2009)
75. J.R. Trail, M.C. Graham, D.M. Bird, Comput. Phys. Commun. **137**, 163 (2001)

76. M. Persson, Phil. Trans. R. Soc. Lond. A **362**, 1173 (2004)
77. A.C. Luntz, M. Persson, J. Chem. Phys. **123**, 074704 (2005)
78. A.C. Luntz, M. Persson, S. Wagner, C. Frischkorn, M. Wolf, J. Chem. Phys. **124**, 244702 (2006)
79. J.R. Trail, M.C. Graham, D.M. Bird, M. Persson, S. Holloway, Phys. Rev. Lett. **88**, 166802 (2002)
80. J.R. Trail, D.M. Bird, M. Persson, S. Holloway, J. Chem. Phys. **119**, 4539 (2003)
81. M. Timmer, P. Kratzer, Phys. Rev. B **79**, 165407 (2009)
82. M. Timmer, P. Kratzer, Surf. Sci. **604**, 1452 (2010)
83. M. Grotemeyer, E. Pehlke, Ab-initio Molecular Dynamics Simulation of Electronic Energy Dissipation: HCl/Al(111) (2010)
84. H. Nienhaus, Chemicurrents are not detectable during Adsorption of Molecular Oxygen on Palladium Surfaces (2009)
85. I. Goikoetxea, J. Beltrán, J. Meyer, M. Alducin, J.I. Juaristi, K. Reuter, New J. Phys. **14**, 013050 (2012)
86. A. Hellman, B. Razaznejad, Y. Yourdshahyan, H. Ternow, I. Zorić, B. Lundqvist, Surf. Sci. **532535**, 126 (2003)
87. A. Hellman, Phys. Rev. B **72**, 201403 (2005)
88. A. Hellman, B. Razaznejad, B.I. Lundqvist, Phys. Rev. B **71**, 205424 (2005)
89. J.C. Polanyi, R.J. Wolf, J. Chem. Phys. **82**, 1555 (1985)
90. J.C. Tully, J. Chem. Phys. **73**, 1975 (1980)
91. H.J. Freund, Surf. Sci. **500**, 271 (2002)
92. H.A. Gasteiger, S.S. Kocha, B. Sompalli, F.T. Wagner, Appl. Catal. B **56**, 9 (2005)
93. A.C. Luntz, M.D. Williams, D.S. Bethune, J. Chem. Phys. **89**, 4381 (1988)
94. W. Wurth, J. Stöhr, P. Feulner, X. Pan, K.R. Bauchspiess, Y. Baba, E. Hudel, G. Rocker, D. Menzel, Phys. Rev. Lett. **65**, 2426 (1990)
95. C.T. Rettner, C.B. Mullins, J. Chem. Phys. **94**, 1626 (1991)
96. J. Wintterlin, R. Schuster, G. Ertl, Phys. Rev. Lett. **77**, 123 (1996)
97. B.C. Stipe, M.A. Rezaei, W. Ho, S. Gao, M. Persson, B.I. Lundqvist, Phys. Rev. Lett. **78**, 4410 (1997)
98. P.D. Nolan, B.R. Lutz, P.L. Tanaka, J.E. Davis, C.B. Mullins, Phys. Rev. Lett. **81**, 3179 (1998)
99. P.D. Nolan, B.R. Lutz, P.L. Tanaka, J.E. Davis, C.B. Mullins, J. Chem. Phys. **111**, 3696 (1999)
100. P. Gambardella, Ž. Šljivančanin, B. Hammer, M. Blanc, K. Kuhnke, K. Kern, Phys. Rev. Lett. **87**, 056103 (2001)
101. H. Steininger, S. Lehwald, H. Ibach, Surf. Sci. **123**, 1 (1982)
102. C. Puglia, A. Nilsson, B. Hernnäs, O. Karis, P. Bennich, N. Mårtensson, Surf. Sci. **342**, 119 (1995)
103. A. Eichler, J. Hafner, Phys. Rev. Lett. **79**, 4481 (1997)
104. A. Eichler, F. Mittendorfer, J. Hafner, Phys. Rev. B **62**, 4744 (2000)
105. F. Kirchhoff, M.J. Mehl, N.I. Papanicolaou, D.A. Papaconstantopoulos, F.S. Khan, Phys. Rev. B **63**, 195101 (2001)
106. A. Groß, A. Eichler, J. Hafner, M.J. Mehl, D.A. Papaconstantopoulos, Surf. Sci. **539**, L542 (2003)
107. A. Groß, A. Eichler, J. Hafner, M.J. Mehl, D.A. Papaconstantopoulos, J. Chem. Phys. **124**, 174713 (2006)
108. A. Groß, S. Wilke, M. Scheffler, Phys. Rev. Lett. **75**, 2718 (1995)
109. A. Groß, Appl. Phys. A **67**, 627 (1998)
110. A. Groß, A. Dianat, Phys. Rev. Lett. **98**, 206107 (2007)
111. A. Groß, J. Chem. Phys. **135**, 174707 (2011)
112. Ž. Šljivančanin, B. Hammer, Surf. Sci. **515**, 235 (2002)
113. H.F. Busnengo, W. Dong, P. Sautet, A. Salin, Phys. Rev. Lett. **87**, 127601 (2001)
114. G.J. Kroes, Science **321**, 794 (2008)
115. M. Hand, J. Harris, J. Chem. Phys. **92**, 7610 (1990)
116. M. Dohle, P. Saalfrank, Surf. Sci. **373**, 95 (1997)

117. M. Bonfanti, C. Diaz, M.F. Somers, G.J. Kroes, Phys. Chem. Chem. Phys. **13**, 4552 (2011)
118. B. Jackson, Chem. Phys. Lett. **270**, 484 (1997)
119. M. Nest, P. Saalfrank, J. Chem. Phys. **113**, 8753 (2000)
120. B. Lepetit, D. Lemoine, Z. Medina, B. Jackson, J. Chem. Phys. **134**, 114705 (2011)
121. M.D. Stiles, J.W. Wilkins, M. Persson, Phys. Rev. B **34**, 4490 (1986)
122. J.R. Manson, *Energy Transfer to Phonons in Atom and Molecule Collisions with Surfaces* (Elsevier, 2008), *Handbook of Surface Science*, vol. 3, 1st edn., chap. 3, pp. 53 – 94
123. B. Jackson, J. Chem. Phys. **108**, 1131 (1998)
124. M. Nest, P. Saalfrank, Chem. Phys. **268**, 65 (2001)
125. M.D. Stiles, J.W. Wilkins, Phys. Rev. B **37**, 7306 (1988)
126. M.E. Tuckerman, G.J. Martyna, J. Phys. Chem. B **104**, 159 (2000)
127. H. Lin, D. Truhlar, Theor Chem Acc **117**, 185 (2007)
128. M.I. Baskes, Phys. Rev. B **46**, 2727 (1992)
129. J. Meyer, K. Reuter, *"QM/Me" - a Novel Embedding Scheme for Adsorbate Dynamics on Metal Surfaces*, to be published (2012)
130. A. Groß, **103**, 246101 (2009)
131. H. Brune, J. Wintterlin, J. Trost, G. Ertl, J. Wiechers, R.J. Behm, J. Chem. Phys. **99**, 2128 (1993)
132. S. Schintke, S. Messerli, K. Morgenstern, J. Nieminen, W.D. Schneider, J. Chem. Phys. **114**, 4206 (2001)
133. C. Engdahl, G. Wahnström, Surf. Sci. **312**, 429 (1994)
134. J. Jacobsen, B. Hammer, K.W. Jacobsen, J.K. Nørskov, Phys. Rev. B **52**, 14954 (1995)
135. R. Heid, K.P. Bohnen, Physics Reports **387**, 151 (2003)
136. J. Meyer, K. Reuter, *Chemical Reaction Dynamics on Metal Surfaces – Role of Phonons*, to be published (2012)
137. M.D. Stiles, J.W. Wilkins, Phys. Rev. Lett. **54**, 595 (1985)
138. B. Jackson, Chem. Phys. Lett. **308**, 456 (1999)
139. B. Lepetit, B. Jackson, Phys. Rev. Lett. **107**, 236102 (2011)